A New Look at the Structural and Magnetic Properties of Potassium Neptunate K_2NpO_4 Combining XRD, XANES Spectroscopy, and Low-Temperature Heat Capacity

Smith, Anna L.; Colineau, Eric; Griveau, Jean Christophe; Popa, Karin; Kauric, Guilhem; Martin, Philippe M.; Scheinost, Andreas C.; Cheetham, Anthony K.; Konings, Rudy J.M.

DOI
10.1021/acs.inorgchem.7b00462

Publication date
2017

Document Version
Final published version

Published in
Inorganic Chemistry: including bioinorganic chemistry

Inorganic Chemistry

Article

pubs.acs.org/IC

A New Look at the Structural and Magnetic Properties of Potassium Neptunate K_2NpO_4 Combining XRD, XANES Spectroscopy, and Low-Temperature Heat Capacity

Anna L. Smith,*[,†] Eric Colineau,[‡] Jean-Christophe Griveau,[‡] Karin Popa,[‡] Guilhem Kauric,[§] Philippe Martin,[∥] Andreas C. Scheinost,[⊥] Anthony K. Cheetham,[#] and Rudy J. M. Konings[‡]

[†]Delft University of Technology, Radiation Science & Technology Department, Nuclear Energy and Radiation Applications (NERA), Mekelweg 15, 2629 JB Delft, The Netherlands

[‡]European Commission, DG Joint Research Centre-JRC, Directorate G-Nuclear Safety & Security, Postfach 2340, D-76125 Karlsruhe, Germany

[§]Chimie-ParisTech, ENSCP, 11 Rue Pierre et Marie Curie, 75005 Paris, France

[∥]CEA Marcoule, CEA, DEN, DMRC/SFMA/LCC, F-30207 Bagnols-sur-Cèze Cedex, France

[⊥]Helmholtz Zentrum Dresden Rossendorf (HZDR), Institute of Resource Ecology, P.O. Box 10119, 01314 Dresden, Germany

[#]Department of Materials Science and Metallurgy, University of Cambridge, 27 Charles Babbage Road, Cambridge CB3 0FS, United Kingdom

Supporting Information

ABSTRACT: The physicochemical properties of the potassium neptunate K_2NpO_4 have been investigated in this work using X-ray diffraction, X-ray absorption near edge structure (XANES) spectroscopy at the Np-L_3 edge, and low-temperature heat capacity measurements. A Rietveld refinement of the crystal structure is reported for the first time. The Np(VI) valence state has been confirmed by the XANES data, and the absorption edge threshold of the XANES spectrum has been correlated to the Mössbauer isomer shift value reported in the literature. The standard entropy and heat capacity of K_2NpO_4 have been derived at 298.15 K from the low-temperature heat capacity data. The latter suggest the existence of a magnetic ordering transition around 25.9 K, most probably of the ferromagnetic type.

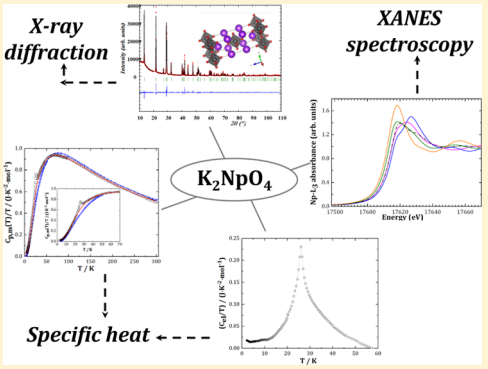

INTRODUCTION

The alkali and alkaline-earth ternary oxides of uranium, neptunium, and plutonium have attracted interest since the 1960s because of their exciting and intriguing electronic and magnetic properties.[1,2] In these systems with $[Rn]6d^15f^n$ (uranium and neptunium) and $[Rn]6d^05f^n$ (plutonium) electronic configurations, the 5f valence shell electrons have a large spatial extension and are close in energy to the 6d electrons, making them prone to chemical bonding, in contrast with the 4f electrons of the lanthanides, which are more core-like. This character leads to a wide range of oxidation states, between +3 and +7, and the occurrence of magnetic ordering behavior. The theoretical description of these systems appears extremely challenging, however, as the crystal field interaction is usually of the same order of magnitude as the spin−orbit coupling interaction and electronic repulsion.[3] The crystal-field interaction cannot be treated as a small perturbation of the electronic energy levels as is done for the $[Xe]4f^n$ rare earths.[3] In the case of $[Rn]5f^1$ and $[Rn]5f^0$ electronic configurations, however, the contribution from electronic repulsion is removed, which greatly simplifies the interpretation.

A number of studies have recently been reported on several sodium actinide phases because of their relevance for the safety assessment of sodium-cooled fast reactors (SFRs).[4−7] Those studies have revealed intriguing magnetic properties for the α-$Na_2Np^{VI}O_4$[7] and $Na_4Np^{VI}O_5$[6] compositions and have stressed the need to re-evaluate the Np(VI) crystal-field ground state.

The physical and chemical properties of K_2NpO_4 have been investigated in the present work in an attempt to bring new insights into the complex behavior of Np(VI) phases. Nectoux et al. performed Mössbauer spectroscopy and magnetic susceptibility measurements on this phase in 1981 and reported intriguing results.[8] The authors suggested the occurrence of a first-order magnetic transition at 19.5(5) K as the Mössbauer spectra showed hyperfine splitting below that temperature, with an associated magnetic hyperfine field of 122 T, corresponding to an ordered moment of about 0.6 μ_B. However, their magnetic susceptibility data did not show any sign of an anomaly around 20 K, as could be expected from the Mössbauer results.

Received: February 27, 2017
Published: April 24, 2017

DOI: 10.1021/acs.inorgchem.7b00462
Inorg. Chem. 2017, 56, 5839−5850

Electronic structures can also be probed using X-ray absorption spectroscopy (XAS).[9] Coupling XAS measurements in the high-energy-resolution fluorescence-detection (HERFD) mode with theoretical calculations using the Anderson impurity model, Butorin et al.[9] have recently estimated the crystal field parameters and 5f occupancy in pentavalent $NaUO_3$ ($[Rn]5f^1$) and hexavalent Pb_3UO_6 ($[Rn]5f^0$), revealing a significant covalent character of the chemical bond. The XAS data available on solid actinide compounds with a valence state higher than IV is still very scarce, however, and the relationship between XAS features and electronic density is not fully understood.[10]

In this work, we have synthesized K_2NpO_4 and report for the first time a Rietveld refinement of its crystal structure and XANES spectrum collected at the Np-L_3 edge. The relationship between local coordination environment and shape of the XANES spectrum is discussed, as well as the correlation between the edge absorption threshold of the neptunium XANES spectrum and the isomer shift value measured by ^{237}Np Mössbauer spectroscopy.[8] Moreover, low-temperature heat capacity measurements have been performed to solve the discrepancy regarding the existence of magnetic ordering in this compound.

EXPERIMENTAL METHODS

Sample Preparation and Characterization. K_2NpO_4 and K_2UO_4 were synthesized under oxygen flow and air by reaction between accurately weighed samples of neptunium dioxide ($^{237}NpO_2$, ORNL, Oak Ridge) or uranium dioxide ($^{238}UO_{2.10}$, JRC-Karlsruhe stocks) and potassium carbonate (K_2CO_3, >99%, Baker). The stoichiometric mixtures were heated with intermediate regrinding steps at 1093 K for 22 h and 1073 K for 5 h for the neptunium (green color) and uranium (orange color) compounds, respectively. The purity of the obtained materials was analyzed by X-ray diffraction. No secondary phases were detected.

^{238}U is an α emitter with a very long half-life (4.47 billion years),[11] making it only weakly radioactive. ^{237}Np decays to ^{233}Pa by α emission with a half-life of 2.14 million years. The ^{233}Pa daughter product is a β^- emitter with a very short half-life (27 days) and significant γ dose rate (1.335×10^{-4} (mSv/h)/MBq).[11] The handling of those materials, requiring considerable safety precautions, was therefore done with limited quantities in α gloveboxes.

The X-ray diffraction measurements were carried out using a Bruker D8 X-ray diffractometer mounted in the Bragg–Brentano configuration with a copper tube (40 kV, 40 mA) and a curved Ge monochromator (111), equipped with a LinxEye position-sensitive detector. The data were collected by step scanning in the angle range $10° \leq 2\theta \leq 120°$ over a period of about 8 h. Structural analysis at room temperature was performed by the Rietveld method with the Fullprof2k suite.[12]

XANES. XANES measurements were performed at the Rossendorf BeamLine (ROBL)[13] of the European Synchrotron Radiation Facility (ESRF, Grenoble, France) on the K_2NpO_4 material. Small amounts (5–10 mg) of powdered sample were mixed with boron nitride (BN) in an argon-filled α glovebox and pressed into pellets for the measurements. The storage ring operating conditions were 6.0 GeV and 170–200 mA. A double-crystal monochromator mounted with a Si(111) crystal coupled to collimating and focusing Rh-coated mirrors was used.

XANES spectra were collected at room temperature in transmission mode at the Np-L_3 edge. A step size of 0.5 eV was used in the edge region. The energy E_0 of the edge absorption threshold position was taken at the first inflection point of the spectrum by using the first node of the second derivative. The position of the white-line maximum was selected from the first node of the first derivative. Several acquisitions were performed on the same sample and summed up to improve the signal to noise ratio. Before the scans were averaged, each spectrum was aligned using the XANES spectrum of a metallic yttrium (17038 eV) reference foil located between the second and the third ionization chambers and measured at the same time as the sample. The ATHENA software (Version 0.9.20)[14] was used to remove the background and to normalize the spectra.

Low-Temperature Heat Capacity of K_2NpO_4 and K_2UO_4. Low-temperature heat capacity measurements were performed using thermal relaxation calorimetry[15] with a PPMS (Physical Property Measurement System, Quantum Design) instrument at applied magnetic fields $B = 0$ and 9 T in the temperature ranges $T = 2.1–298.4$ K for K_2NpO_4 and $T = 2.0–312.4$ K for K_2UO_4, respectively. The measurements were carried out on 22.6(5) mg of K_2NpO_4 material encapsulated in Stycast 2850 FT, and the heat capacity contribution of the Stycast was subtracted from the recorded data. A more detailed description of the experimental procedure, which is particularly well adapted to the study of radioactive materials, was given in ref 16. The measurement of K_2UO_4 was done on 33.2(5) mg of material without additional encapsulation in Stycast. The contributions of the sample platform, wires, and grease were deduced by a separate measurement of an addenda curve. Considering the accuracy of the PPMS instrument as estimated by Lashley et al.,[15] the reproducibility of the measurements, and the error introduced by the encapsulation procedure in Stycast of the radioactive neptunium material,[16] the final uncertainty was estimated to be about 1–2% in the middle range of acquisition (10–100 K) and reach about 3% at the lowest temperatures and near room temperature. Self-heating effects coming from the radioactive decay of ^{237}Np were considered but appeared negligible. The use of Stycast is the main contributor to the uncertainties on the heat capacity and entropy values quoted hereafter. The final uncertainty for the uranium material is estimated to be about 1% from 100 to 300 K and reach about 3% at the lowest temperatures.[15]

RESULTS AND DISCUSSION

Structural Refinement. K_2NpO_4 is isostructural with K_2UO_4 and crystallizes with tetragonal symmetry in space group $I4/mmm$. The structure of K_2UO_4 was refined recently on the basis of single-crystal data.[17] The refined cell parameters obtained in the present study, $a = 4.3322(3)$ Å and $c = 13.1881(13)$ Å, are in good agreement with the literature.[17] The refined atomic positions are given in the Supporting Information. A Rietveld refinement for the K_2NpO_4 phase is reported for the first time in this work (Figure 1). The cell parameters obtained are $a = 4.2973(4)$ Å and $c = 13.144(12)$ Å. The refined atomic positions are given in Table 1 and selected bond lengths in Table 2. In this structure, the neptunium cations are 6-fold coordinated, and the octahedra are connected by their equatorial vertices, forming sheets in the (ab) plane (Figure 2a). The potassium cations, in 9-fold coordination, are located between the sheets, holding them together. The NpO_6 octahedra show a neptunyl type of coordination, with two short Np–O1 bonds at 1.84(1) Å in the axial direction and four long Np–O2 bonds at 2.15(1) Å in the equatorial plane (Figure 2b). The presence of a neptunyl configuration is quite common for hexavalent alkali-metal actinide oxide phases. It has been reported already for α-Na_2NpO_4 ($Np–2O_I = 1.762(5)$ Å, $Np–4O_{II} = 2.086(5)$ Å),[7] β-Na_2NpO_4 ($Np–2O_I = 1.90$ Å, $Np–2O_{II} = 2.16$ Å, $Np–2O_{III} = 2.17$ Å)[18] (orthorhombic in space groups $Pbam$ and $Pbca$, respectively), and $BaNpO_4$ ($Np–2O_I = 1.89$ Å, $Np–2O_{II} = 2.10$ Å, $Np–2O_{III} = 2.20$ Å)[19] (orthorhombic in space group $Pbcm$). The unit cell volume in K_2NpO_4 (242.7 Å^3) is smaller than that for K_2UO_4 (247.5 Å^3), which can be related to the decreasing ionic radius along the series of the actinide elements.

XANES. The XANES spectrum of K_2NpO_4 collected at the Np-L_3 edge is shown in Figure 3 together with those of NpO_2, $Na_3Np^VO_4$, α-$Na_2Np^{VI}O_4$, $Na_4Np^{VI}O_5$, and $Na_5Np^{VII}O_6$ reference materials.[10] The valence states of the sodium neptunates

DOI: 10.1021/acs.inorgchem.7b00462
Inorg. Chem. 2017, 56, 5839–5850

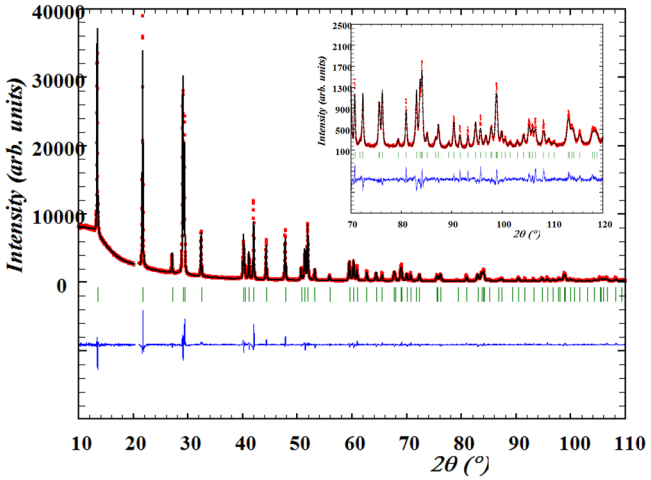

Figure 1. Comparison between the observed (Y_{obs}, in red) and calculated (Y_{calc}, in black) X-ray diffraction patterns of K_2NpO_4 collected at room temperature (T = 295 ± 2 K). $Y_{obs} - Y_{calc}$, in blue, is the difference between the experimental and calculated intensities. The Bragg reflection angular positions are marked in green. The inset shows an enlargement of the refinement in the angle range 2θ = 70−120°. Measurements were carried out with λ = Cu Kα_1 radiation.

Table 1. Refined Atomic Positions in K_2NpO_4 Derived from the Analysis of the X-ray Diffraction Data Collected at Room Temperature (T = 295 ± 2 K)[a]

atom	oxidn state	Wyckoff	x	y	z	B_0 (Å^2)
Np	+6	2a	0	0	0	0.78(1)
K	+1	4e	0.5	0.5	0.1520(2)	1.91(6)
O1	−2	4e	0	0	0.1415(5)	1.5(2)
O2	−2	4c	0.5	0	0	2.1(2)

[a] R_{wp} = 13.5, R_{exp} = 5.37, χ^2 = 6.29.

Table 2. Selected Bond Lengths in M_2AnO_4 (An = U, Np; M = Na, K)[a]

		bond length (Å)		
bond	N	K_2UO_4	K_2NpO_4	α-Na_2NpO_4
An−O1	2	1.812(7)	1.860(7)	1.762(5)
An−O2	4	2.166(1)	2.149(1)	2.086(5)
K−O1	1	2.801(7)	2.714(7)	
K−O1	4	3.068(1)	3.042(1)	
K−O2	4	2.935(2)	2.934(2)	

[a] N is the number of atoms in each coordination shell.

were confirmed by ^{237}Np Mössbauer spectroscopy from the values of their isomer shifts,[5−7] while the corresponding XANES spectra were reported in ref 10. The values of the measured inflection points and white lines are reported in Table 3. The investigated series covered a wide range of oxidation states (IV−VII) and a variety of local coordination geometries around the neptunium cation, i.e., neptunyl (Na_3NpO_4 and α-Na_2NpO_4), "reverse" neptunyl (Na_4NpO_5), and distorted NpO_6 octahedra (Na_5NpO_6), which has allowed us to correlate the shape of the XANES spectra with the local structural environments,[10] as described later in this paper.

The inflection point position of K_2NpO_4, corresponding to the absorption edge threshold E_0 for the 2p → 6d transitions, is well aligned with those of α-$Na_2Np^{VI}O_4$ and $Na_4Np^{VI}O_5$ (Table 3). These results confirm that neptunium is exclusively in the oxidation state VI in K_2NpO_4, corresponding to a [Rn]5f^1 electronic configuration. The Np ion in this structure is therefore a Kramers ion with a $^2F_{5/2}$ ground state manifold, and a $^2F_{7/2}$ first excited state arising from spin−orbit coupling.

Smith et al. reported a linear correlation of the absorption edge threshold E_0 determined by XANES versus the Mössbauer isomer shift for the series of sodium neptunates.[10] The value for K_2NpO_4 fits very well with this trend (Figure 4) when the isomer shift value determined by Nectoux et al. is used: i.e., δ_{IS} = −56.9(6) mm s^{-1} at 4.2 K relative to the standard $NpAl_2$ absorber.[8] The linear variation between E_0 and δ_{IS} can be understood from the fact that both quantities result from the Coulomb interaction with the surrounding electrons. The 5f shells produce a shielding effect on the electronic charge density of the $s_{1/2}$ and $p_{1/2}$ inner shells, which affects the isomer shift: $\delta_{IS} = \alpha[\Delta\rho_e(0)]$ (α being a calibration constant and $\Delta\rho_e(0)$ the difference in electronic charge density between the source material and the absorber at the nuclear origin). $\rho_e(0)$ increases with the removal of 5f electrons. Moreover, the increase in formal valence state produces a decrease in Coulomb energy in the final state between the 5f and 6d electrons and the $2p_{3/2}$ core hole,[20−22] which leads to a shift to higher energy of the absorption edge threshold E_0.

In addition, the XANES spectrum of K_2NpO_4 shows the typical double-peaked white lines (WL) of Np(V), Np(VI), and Np(VII) compounds,[10,20,21] while the tetravalent $Np^{IV}O_2$ compound exhibits a single WL peak. The double peak consists of the main white line at 17620.2(5) eV and a shoulder and reduced peak amplitude about 15 eV above the Np edge. This feature has traditionally been attributed to localized multiple-scattering resonance of the neptunyl configuration. However, studies[10] on the sodium uranates and neptunates have shown that the correlation between the shape of the XANES spectra and the local coordination geometries is probably more intricate. The isostructural compounds α-$Na_2U^{VI}O_4$ and α-$Na_2Np^{VI}O_4$, presenting a neptunyl type of configuration, do not show the expected secondary shoulder and reduced peak amplitude, whereas $Na_4U^{VI}O_5$, presenting a "reverse" neptunyl type of configuration, does.[10] Other factors could play a role, and effects of the degree of localization of the 5f electrons[10] and core-ionized final states with different 5f occupancies[20,21] have been suggested.

The absorption edge threshold E_0 is finally slightly higher (0.3 eV) for K_2NpO_4 than for α-$Na_2Np(VI)O_4$, which could be related to the neptunyl bond distances (Table 2), degree of covalency, or (in other words) degree of localization of the 5f electrons in both compounds. The shorter the Np−O bonds, the more localized the 5f electrons, and the greater the Coulomb energy, making it easier to eject an electron from the $2p_{3/2}$ core−shell. However, it is not possible to conclude definitively, given the experimental uncertainties (0.5 eV) of the measurements at the Np-L_3 edge, and this would require performing high-energy-resolution fluorescence-detected (HERFD) XANES measurements at the M_4 edge.

Heat Capacity Measurements. The heat capacity data of K_2NpO_4 and K_2UO_4 measured at low temperatures in the absence of a magnetic field are shown in Figure 5 and given in Tables 5 and 6 of the Appendix. The two curves cross above T = 150 K, although one would expect them to become equal, corresponding to the same lattice contribution at high temperatures for the uranium and neptunium compounds. However, this discrepancy can be related on the one hand to the uncertainty on our experimental results, which increases toward

DOI: 10.1021/acs.inorgchem.7b00462
Inorg. Chem. 2017, 56, 5839−5850

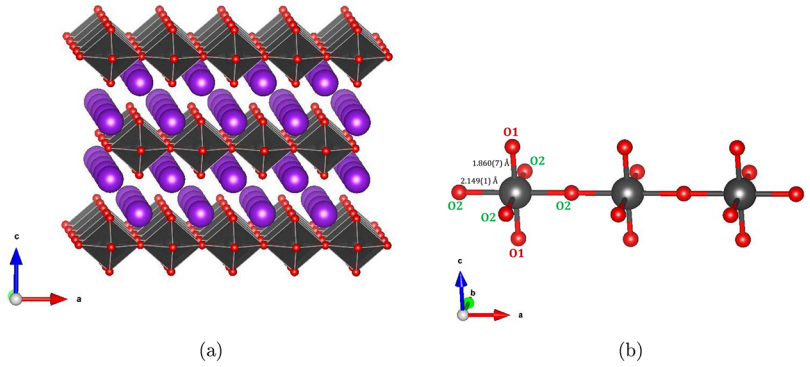

(a) (b)

Figure 2. (a) Crystal structure of K_2NpO_4 (K atoms in purple, O atoms in red, NpO_6 octahedra in gray) showing the sheets of corner-sharing NpO_6 octahedra in the (*ab*) plane. (b) NpO_6 octahedron in K_2NpO_4 with the neptunyl type of coordination.

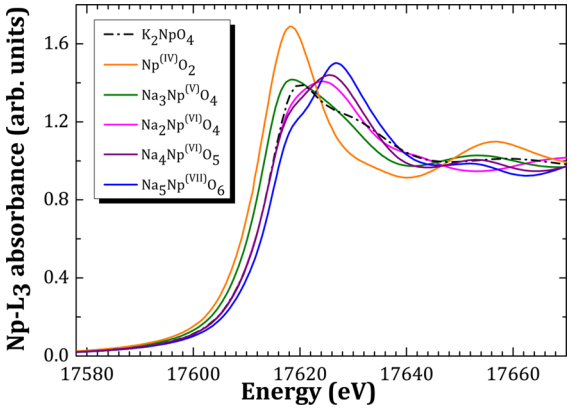

Figure 3. Normalized XANES spectrum of K_2NpO_4 (present work) together with those of NpO_2, Na_3NpO_4, α-Na_2NpO_4, Na_4NpO_5, and Na_5NpO_6 reference materials.[10]

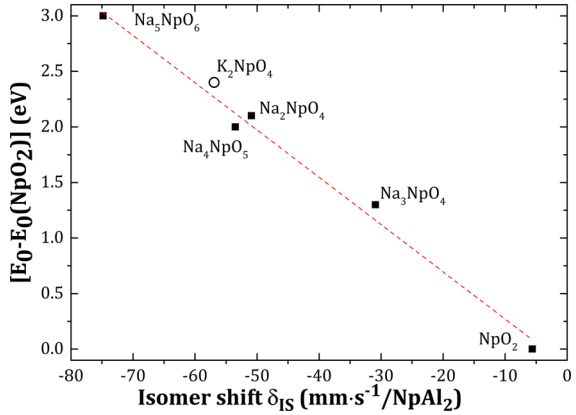

Figure 4. Absorption edge threshold E_0 relative to NpO_2 versus isomer shift measured by Mössbauer spectroscopy.

Table 3. Energies of the Inflection Points and White Lines of the Np-L_3 XANES Spectra[a]

compound	inflection point (eV)	white line (eV)		ref
K_2NpO_4	17614.5(5)	17620.2(5)	*17631.5(5)*	this work
$Np^{IV}O_2$	17612.1(5)	17618.3(5)		10
$Na_3Np^{V}O_4$	17613.4(5)	17618.5(5)		10
α-$Na_2Np^{VI}O_4$	17614.2(5)	17624.3(5)		10
$Na_4Np^{VI}O_5$	17614.1(5)	17618.8(5)	17625.6(5)	10
$Na_5Np^{VII}O_6$	17615.1(5)	*17619.0(5)*	17626.9(5)	10

[a]The secondary white line, if present, is given in italics.

high temperatures using the PPMS technique, and on the other hand to the fact that one compound was measured with Stycast and the other without. The uncertainty on the neptunium data corrected for the Stycast contribution is around 3% at room temperature, whereas that of the uranium data measured without Stycast is around 1%. The heat capacities reach values that are about 17−24 J K^{-1} mol^{-1} below the classical Dulong−Petit limit ($C_{lat} = 21R \approx 174.6$ J K^{-1} mol^{-1} for the seven atoms in the formula unit) as the temperature approaches 298.15 K.

The collected data for K_2NpO_4 show a small anomaly at T = 25.9 K, which is almost unaffected by the application of a 9 T magnetic field apart from a small decrease in the amplitude. This feature could be interpreted at first as an indication of the presence of NpO_2 impurity within the investigated material. Indeed, neptunium dioxide shows a sharp λ anomaly at

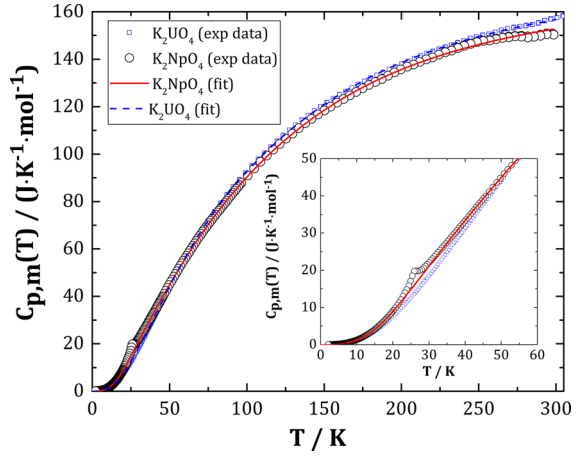

Figure 5. Heat capacity of K_2NpO_4 (black ○) and K_2UO_4 (blue □) measured in zero magnetic field and the numerical fit to the neptunium (red line) and uranium (blue dotted line) data.

T = 25.7 K[23,24] due to rank 5 triacontadipolar order as described in the studies of Santini et al.,[25] with a similar behavior upon application of a magnetic field. However, the X-ray diffraction data did not reveal any secondary NpO_2 phase. Moreover, the shape of the anomaly in K_2NpO_4 does not match that of NpO_2, although the critical temperatures are very close. The anomaly is very symmetrical in K_2NpO_4, in contrast with NpO_2, showing an asymmetrical profile. On the basis of its amplitude, the amount of NpO_2 impurity would correspond to 26.9 ± 1.0%, which should be detected easily by the X-rays.

DOI: 10.1021/acs.inorgchem.7b00462
Inorg. Chem. 2017, 56, 5839−5850

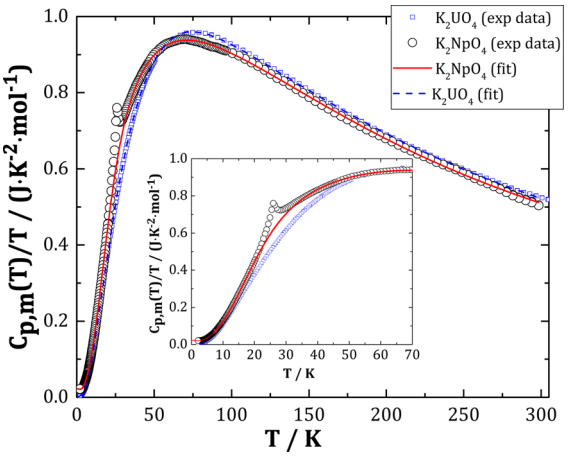

Figure 6. C_p/T for K_2NpO_4 (black ○) and K_2UO_4 (blue □) measured in zero magnetic field and the numerical fit to the neptunium (red line) and uranium (blue dotted line) data.

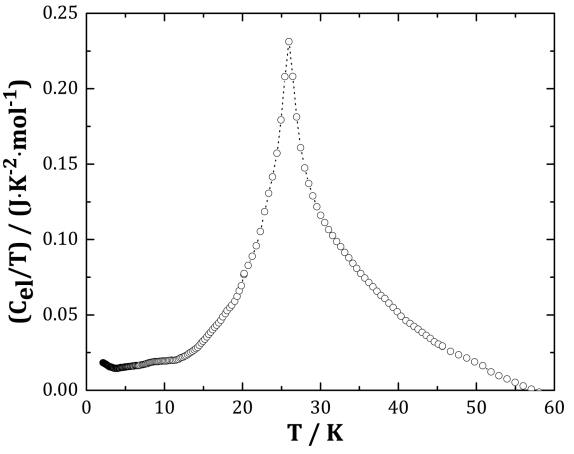

Figure 7. Electronic contribution to the heat capacity in K_2NpO_4 obtained by subtracting the data for K_2UO_4.

We conclude that the anomaly is an intrinsic property of K_2NpO_4. The corresponding magnetic contribution was derived as S_{mag} = 3.1 ± 0.1 J K^{-1} mol^{-1} after subtraction of the lattice heat capacity contribution (Figure 7). The latter was approximated with the heat capacity of K_2UO_4 (which has electronic configuration [Rn]$5f^0$), as the two compounds are isostructural and have very similar atomic masses. The derived magnetic entropy value represents about 53.8% of the expected order−disorder entropy for such a Kramers system (S_{mag} = Rln2). It is worth pointing out that a low magnetic entropy, i.e. 0.19Rln2, has also been reported for α-Na_2NpO_4.[7]

Interestingly, no anomaly was observed around 19.5(5) K, as could be expected from the Mössbauer results of Nectoux et al.[8] An X-ray diffraction pattern collected after the low-temperature heat capacity measurement moreover confirmed that the sample had retained its integrity during the experiment. Since the magnetic susceptibility measurements of the authors also did not show any anomaly around 20 K,[8] the existence of a first-order magnetic phase transition at the latter temperature is unlikely. To explain the origin of the magnetic hyperfine splitting reported below 19.5(5) K, we could suggest the occurrence of a slow electron spin relaxation phenomenon in this paramagnetic system.[26] However, this is doubtful, as it would require a sudden collapse of the relaxation time at the critical temperature. The cell parameters reported by[8] for K_2NpO_4 (a = 4.26 Å and c = 13.01 Å) are lower than those found in this study. A contamination of their sample with a magnetic impurity is possible although unlikely, as they reported a single-phase material, but they give very little detail on phase preparation and purity. The magnetic hyperfine splitting effect observed by the authors probably corresponds to the anomaly observed herein at 25.9 K, with a somewhat lower critical temperature. It should be pointed out that differences in critical temperatures of about 3−8 K have been reported in the literature between Mössbauer and magnetic susceptibility results of the uranium−neptunium mixed oxides $U_{1-x}Np_xO_2$.[27] For the magnetic susceptibilty results of Nectoux et al., a clear deviation from the Curie−Weiss law is observed below about 40 K, which could suggest ferromagnetic ordering below the latter temperature. The hypothesis of a ferromagnetic transition is moreover in good agreement with the low-temperature heat

Table 4. Summary of Fitting Parameters of the Heat Capacities of K_2NpO_4 and K_2UO_4

Debye and Einstein fit		harmonic lattice model	
		K_2NpO_4	
temp range/K	7.71−298.4	temp range/K	2.1−8.0
n_D/mol	2.3637	δ/mJ mol^{-1} K^{-1}	22.25
Θ_D/K	154.41	B_3/mJ mol^{-1} K^{-4}	-5.00553×10^{-1}
n_{E1}/mol	1.9806	B_5/mJ mol^{-1} K^{-6}	6.48526×10^{-2}
Θ_{E1}/K	588.19	B_7/mJ mol^{-1} K^{-8}	-1.13475×10^{-3}
n_{E2}/mol	2.5292	B_9/mJ mol^{-1} K^{-10}	7.32029×10^{-6}
θ_{E2}/K	287.56		
$n_D + n_{E1} + n_{E2}$ mol	6.87		
		K_2UO_4	
temp range/K	19.8−312.4	temp range/K	2.0−20.3
n_D/mol	2.0522	δ/mJ mol^{-1} K^{-1}	
Θ_D/K	157.08	B_3/mJ mol^{-1} K^{-4}	6.43253×10^{-1}
n_{E1}/mol	2.8798	B_5/mJ mol^{-1} K^{-6}	7.77235×10^{-3}
Θ_{E1}/K	256.28	B_7/mJ mol^{-1} K^{-8}	-4.50504×10^{-5}
n_{E2}/mol	2.1601	B_9/mJ mol^{-1} K^{-10}	1.03519×10^{-7}
Θ_{E2}/K	610.54	B_{11}/mJ mol^{-1} K^{-12}	-8.70422×10^{-11}
$n_D + n_{E1} + n_{E2}$/mol	7.09		

DOI: 10.1021/acs.inorgchem.7b00462
Inorg. Chem. 2017, 56, 5839−5850

Table 5. Experimental Heat Capacity Data for K_2NpO_4

T (K)	$C_{p,m}$ (J K^{-1} mol^{-1})	T (K)	$C_{p,m}$ (J K^{-1} mol^{-1})	T (K)	$C_{p,m}$ (J K^{-1} mol^{-1})	T (K)	$C_{p,m}$ (J K^{-1} mol^{-1})
298.43	150.54	85.02	78.554	24.42	15.844	6.48	0.34949
294.03	150.86	83.99	77.755	23.85	14.756	6.37	0.33499
289.93	150.33	82.96	76.911	23.36	13.900	6.28	0.32159
285.82	149.69	81.93	76.129	22.84	12.998	6.18	0.30762
281.73	149.58	80.89	75.293	22.31	12.091	6.08	0.29390
277.63	149.82	79.86	74.402	21.78	11.282	5.99	0.28239
273.52	149.74	78.83	73.565	21.27	10.562	5.89	0.27128
269.43	149.51	77.80	72.677	20.75	9.8837	5.80	0.26038
265.33	149.08	76.76	71.782	20.23	9.2323	5.71	0.24960
261.22	148.55	75.72	70.859	20.20	9.1766	5.62	0.23952
257.14	148.02	74.66	69.965	19.87	8.7947	5.54	0.22983
253.02	147.74	73.63	69.067	19.61	8.4794	5.45	0.22093
248.91	147.34	72.58	68.161	19.33	8.1474	5.37	0.21260
244.82	146.52	71.55	67.253	19.02	7.7921	5.28	0.20444
240.71	145.80	70.52	66.326	18.63	7.3831	5.20	0.19678
236.60	144.76	69.46	65.342	18.40	7.1413	5.12	0.18957
232.49	143.72	68.45	64.351	18.05	6.7913	5.05	0.18253
228.38	142.94	67.37	63.336	17.83	6.5588	4.97	0.17529
224.26	141.92	66.36	62.325	17.50	6.2451	4.89	0.16922
298.44	150.31	65.33	61.283	17.26	6.0007	4.81	0.16271
294.01	150.46	64.29	60.232	16.98	5.7453	4.74	0.15676
289.93	149.89	63.28	59.191	16.71	5.5090	4.67	0.15113
285.82	149.43	62.21	58.128	16.46	5.2871	4.59	0.14569
281.73	149.17	61.19	57.077	16.19	5.0570	4.53	0.14069
277.62	149.45	60.14	56.013	15.93	4.8413	4.46	0.13668
273.52	149.59	59.11	54.951	15.69	4.6426	4.40	0.13278
269.43	149.21	58.06	53.886	15.44	4.4386	4.33	0.12729
265.34	148.96	57.04	52.797	15.20	4.2445	4.27	0.12352
261.22	148.37	56.01	51.691	14.96	4.0631	4.21	0.11882
257.14	147.86	54.98	50.565	14.73	3.8884	4.14	0.11501
253.02	147.68	53.93	49.409	14.49	3.7147	4.08	0.11167
248.92	147.15	52.89	48.237	14.26	3.5466	4.02	0.10681
244.82	146.41	51.87	47.086	14.04	3.3925	3.96	0.10417
240.71	145.63	50.82	45.966	13.82	3.2445	3.90	0.10116
236.61	144.68	49.78	44.771	13.60	3.1012	3.84	9.8110×10^{-2}
232.49	143.61	48.75	43.566	13.39	2.9653	3.78	9.5240×10^{-2}
228.38	142.92	47.74	42.347	13.18	2.8324	3.73	9.2290×10^{-2}
224.29	141.89	46.70	41.101	12.97	2.7042	3.68	9.0240×10^{-2}
220.16	140.75	45.66	39.889	12.77	2.5822	3.61	8.7210×10^{-2}
216.06	139.89	45.66	39.880	12.57	2.4684	3.56	8.5010×10^{-2}
211.94	138.80	45.12	39.234	12.37	2.3554	3.51	8.3120×10^{-2}
207.84	137.72	44.60	38.616	12.18	2.2514	3.46	8.1080×10^{-2}
203.72	136.85	44.08	38.031	11.99	2.1480	3.41	7.9860×10^{-2}
199.59	135.65	43.57	37.429	11.80	2.0471	3.37	7.8210×10^{-2}
195.49	134.41	43.05	36.821	11.61	1.9534	3.32	7.6230×10^{-2}
191.37	132.98	42.53	36.209	11.43	1.8609	3.27	7.4610×10^{-2}
187.26	131.58	42.01	35.596	11.24	1.7761	3.23	7.3660×10^{-2}
183.14	130.38	41.50	34.980	11.07	1.6978	3.18	7.1800×10^{-2}
179.02	129.08	40.96	34.338	10.89	1.6220	3.13	7.0580×10^{-2}
174.90	127.64	40.34	33.623	10.72	1.5477	3.08	6.8430×10^{-2}
170.78	126.15	39.85	33.082	10.56	1.4775	3.04	6.7060×10^{-2}
166.67	124.67	39.32	32.475	10.39	1.4086	3.00	6.5610×10^{-2}
162.55	123.14	38.80	31.875	10.23	1.3448	2.95	6.4510×10^{-2}
158.43	121.57	38.28	31.284	10.07	1.2850	2.91	6.3420×10^{-2}
154.30	120.01	37.77	30.678	9.91	1.2273	2.88	6.2390×10^{-2}
150.18	118.35	37.27	30.103	9.76	1.1717	2.84	6.1410×10^{-2}
146.05	116.73	36.74	29.492	9.61	1.1175	2.80	6.0530×10^{-2}
141.92	114.85	36.23	28.901	9.46	1.0665	2.76	5.9840×10^{-2}
137.79	112.97	35.70	28.300	9.31	1.0164	2.73	5.8780×10^{-2}
133.66	110.94	35.19	27.709	9.16	0.97051	2.69	5.8210×10^{-2}
129.51	108.52	34.67	27.125	9.02	0.92699	2.65	5.7300×10^{-2}

DOI: 10.1021/acs.inorgchem.7b00462
Inorg. Chem. 2017, 56, 5839−5850

Table 5. continued

T (K)	$C_{p,m}$ (J K^{-1} mol^{-1})	T (K)	$C_{p,m}$ (J K^{-1} mol^{-1})	T (K)	$C_{p,m}$ (J K^{-1} mol^{-1})	T (K)	$C_{p,m}$ (J K^{-1} mol^{-1})
125.39	106.47	34.16	26.554	8.88	0.88453	2.62	5.6670×10^{-2}
121.26	104.23	33.64	25.977	8.74	0.84464	2.58	5.5870×10^{-2}
117.14	101.86	33.12	25.399	8.61	0.80641	2.55	5.4840×10^{-2}
113.00	99.342	32.61	24.834	8.47	0.76952	2.52	5.4310×10^{-2}
108.85	96.705	32.10	24.250	8.34	0.73372	2.49	5.3670×10^{-2}
104.73	93.925	31.58	23.682	8.21	0.70041	2.46	5.2780×10^{-2}
100.59	90.936	31.07	23.119	8.08	0.66801	2.43	5.2170×10^{-2}
96.44	87.774	30.55	22.574	7.96	0.63753	2.40	5.1490×10^{-2}
96.49	87.826	30.05	22.049	7.83	0.60685	2.37	5.0650×10^{-2}
95.35	86.884	29.56	21.568	7.71	0.57981	2.34	5.0040×10^{-2}
94.31	86.108	29.03	21.068	7.59	0.55302	2.31	4.9240×10^{-2}
93.28	85.263	28.51	20.624	7.48	0.52777	2.28	4.8980×10^{-2}
92.24	84.467	28.00	20.227	7.36	0.50407	2.26	4.8450×10^{-2}
91.22	83.658	27.48	19.908	7.25	0.48099	2.23	4.7590×10^{-2}
90.19	82.867	26.95	19.755	7.13	0.45942	2.21	4.7150×10^{-2}
89.16	82.003	26.47	19.827	6.93	0.42253	2.18	4.6610×10^{-2}
88.12	81.115	25.96	19.738	6.78	0.39766	2.16	4.6260×10^{-2}
87.08	80.204	25.46	18.459	6.68	0.38007	2.13	4.5250×10^{-2}
86.05	79.395	24.95	17.054	6.58	0.36403		

capacity data, showing a slight decrease of the anomaly at T = 25.9 K upon application of a magnetic field. The negative value of the Curie constant, i.e., Θ_P = −150 K, derived from the Curie−Weiss analysis of the data[8] is rather surprising, however. It suggests a more complex order, possibly with a canting of the ferromagnetically coupled moments or with strong antiferromagnetic interactions.

In the present work, the thermodynamic functions of K_2NpO_4 and K_2UO_4 were derived at 298.15 K by fitting the experimental data to theoretical functions below T = 8.0 K and T = 20.0 K,[28] respectively, and a combination of Debye and Einstein heat capacity functions[29−31] at T = 7.8−298.4 K and at T = 20.0−312.4 K, respectively. The fitted data are shown with solid and dotted lines in Figures 5 and 6. The heat capacity values at 298.15 K were obtained by interpolation, yielding $C_{p,m}^{\circ}(K_2NpO_4, cr, 298.15\ K)$ = 152.7 ± 4.5 J K^{-1} mol^{-1} and $C_{p,m}^{\circ}(K_2UO_4, cr, 298.15\ K)$ = 156.5 ± 1.6 J K^{-1} mol^{-1} (in both cases, the quoted uncertainty corresponds to the standard uncertainty). The experimental standard entropies at 298.15 K were determined by numerical integration of $C_{p,m}/T = f(T)$ using the aforementioned fitted functions and including the magnetic entropy contribution, yielding $S_m^{\circ}(K_2NpO_4, cr, 298.15\ K)$ = 209.3 ± 4.9 J K^{-1} mol^{-1} and $S_m^{\circ}(K_2UO_4, cr, 298.15\ K)$ = 210.1 ± 2.7 J K^{-1} mol^{-1}, respectively. The values obtained for K_2NpO_4 are slightly lower than that of K_2UO_4, whereas the inverse behavior would be expected. However, this is due to the uncertainty introduced by the use of Stycast as mentioned before and the crossing of the two curves. When adding the derived magnetic entropy to the lattice contribution of K_2UO_4, one derives 213.2 J K^{-1} mol^{-1} for the standard entropy of K_2NpO_4, which remains within the uncertainty of the present measurement.

Fitting of the Lattice Contribution above T = 8.0 K (K_2NpO_4) and T = 20.0 K (K_2UO_4). At very low temperatures where the thermal expansion is negligible, the heat capacity at constant pressure can be approximated to the heat capacity at constant volume $C_{p,m} \approx C_{V,m}$, which comprises lattice vibrations, electronic, and magnetic contributions[32]

The lattice contribution dominates at temperatures above about T = 8−20 K and can be modeled using a combination of Debye and Einstein functions, as shown in eq 1. Two Einstein functions were used in this work to fit the data. Fitting with a single Einstein function was attempted but could not reproduce accurately the high-temperature region:

$$C_{p,m} = n_D D(\Theta_D) + n_{E1} E(\Theta_{E1}) + n_{E2} E(\Theta_{E2}) \quad (1)$$

where R is the universal gas constant equal to 8.3144621 J K^{-1} mol^{-1}, $D(\Theta_D)$, $E(\Theta_{E1})$, and $E(\Theta_{E2})$ are the Debye and Einstein functions, respectively, as written in eqs 2 and 3. Θ_D, Θ_{E1}, and Θ_{E2} are the characteristic Debye and Einstein temperatures. n_D, n_{E1}, and n_{E2} are adjustable parameters, whose sum $n_D + n_{E1} + n_{E2}$ should be approximately equal to the number of atoms in the formula unit (i.e., 7 in this case).

$$D(\Theta_D) = 9R\left(\frac{1}{x}\right)^3 \int_0^x \frac{e^x x^4}{[e^x - 1]^2}\,dx \qquad x = \frac{\Theta_D}{T} \quad (2)$$

$$E(\Theta_E) = 3Rx^2 \frac{e^x}{[e^x - 1]^2} \qquad x = \frac{\Theta_E}{T} \quad (3)$$

The fitted parameters are listed in Table 4. The sum $n_D + n_{E1} + n_{E2}$ is very close to 7.

Fitting below T = 8.0 K (K_2NpO_4) and T = 20.0 K (K_2UO_4). At very low temperatures (T < 20 K), the phonon contribution is well-represented using a harmonic lattice model,[28] as expressed by the polynomial function (4), where the number of required terms augments the high-temperature limit of the fit:

$$C_{latt} = \sum B_n T^n \qquad n = 3, 5, 7, 9, 11 \ldots \quad (4)$$

The electronic contribution of the conduction electrons at the Fermi surface are represented with the linear term γT.[33] For insulating materials such as K_2NpO_4 and K_2UO_4, the electronic specific heat is 0. However, a linear term was reported in materials such as α-FeOOH,[28] $Fe_3(P_2O_7)_2$,[34] and $Sr_2TiSi_2O_8$,[35] which was related to departure from stoichiometry, oxygen vacancies, or defects within the material.[28]

The heat capacity of K_2NpO_4 was fitted with the harmonic model using four terms over the temperature range T = 2.1−8.0 K. That of K_2UO_4 was fitted with five terms over

DOI: 10.1021/acs.inorgchem.7b00462
Inorg. Chem. 2017, 56, 5839−5850

Table 6. Experimental Heat Capacity Data for K_2UO_4

T (K)	$C_{p,m}$ (J K^{-1} mol^{-1})	T (K)	$C_{p,m}$ (J K^{-1} mol^{-1})	T (K)	$C_{p,m}$ (J K^{-1} mol^{-1})	T (K)	$C_{p,m}$ (J K^{-1} mol^{-1})
312.40	161.60	87.12	82.810	27.38	15.298	7.48	0.39842
312.39	160.58	87.12	82.832	26.87	14.665	7.48	0.39873
312.43	160.24	83.06	79.366	26.88	14.708	7.49	0.39950
308.36	159.08	83.08	79.371	26.88	14.710	7.31	0.36697
308.60	159.45	83.07	79.384	26.36	14.113	7.31	0.36579
308.62	159.18	79.01	75.676	26.37	14.124	7.31	0.36601
304.47	158.20	79.03	75.691	26.36	14.118	7.13	0.33632
304.70	158.39	79.03	75.666	25.85	13.545	7.14	0.33672
304.69	158.12	74.96	71.826	25.86	13.552	7.14	0.33674
300.55	157.42	74.98	71.838	25.86	13.538	6.99	0.31321
300.75	157.55	74.97	71.820	25.35	12.967	6.99	0.31255
300.73	157.45	70.92	67.795	25.36	12.993	6.99	0.31434
296.58	156.80	70.93	67.829	25.35	12.988	6.81	0.28615
296.75	157.07	70.93	67.795	24.84	12.425	6.82	0.28738
296.76	156.87	66.87	63.596	24.85	12.432	6.82	0.28696
292.59	156.14	66.89	63.611	24.85	12.431	6.65	0.26296
292.77	156.35	66.88	63.570	24.33	11.897	6.66	0.26242
292.78	156.33	62.82	59.113	24.34	11.883	6.66	0.26271
288.60	155.09	62.84	59.113	24.34	11.875	6.50	0.24180
288.78	155.43	62.84	59.100	23.83	11.364	6.50	0.24290
288.76	155.30	58.78	54.552	23.84	11.333	6.50	0.24231
284.60	154.49	58.79	54.568	23.83	11.327	6.34	0.22326
284.76	154.64	58.79	54.563	23.32	10.786	6.35	0.22277
284.75	154.60	54.74	49.801	23.33	10.798	6.35	0.22412
280.59	154.01	54.75	49.816	23.33	10.789	6.20	0.20715
280.75	154.35	54.74	49.793	22.81	10.294	6.20	0.20732
280.74	154.15	50.69	44.917	22.82	10.275	6.20	0.20594
276.58	153.78	50.70	44.927	22.82	10.262	6.05	0.18998
276.73	153.87	50.69	44.910	22.31	9.7523	6.05	0.19010
276.73	153.81	50.71	44.955	22.31	9.7381	6.06	0.19027
272.57	153.15	50.69	44.922	22.31	9.7462	5.91	0.17522
272.73	153.46	50.69	44.898	21.80	9.2319	5.91	0.17396
272.71	153.29	50.16	44.249	21.80	9.2338	5.91	0.17499
268.56	152.73	50.19	44.281	21.80	9.2329	5.77	0.16011
268.70	152.83	50.19	44.279	21.30	8.7270	5.77	0.16012
268.70	152.83	49.66	43.617	21.30	8.7410	5.78	0.16111
264.55	152.10	49.68	43.655	21.30	8.7381	5.64	0.14760
264.67	152.31	49.68	43.657	20.79	8.2552	5.64	0.14831
264.68	152.29	49.15	42.987	20.79	8.2590	5.64	0.14809
260.53	151.17	49.18	43.031	20.79	8.2572	5.50	0.13636
260.65	151.44	49.17	43.034	20.28	7.7823	5.51	0.13711
260.65	151.42	48.65	42.348	20.29	7.7952	5.51	0.13768
256.51	150.55	48.67	42.386	20.28	7.7825	5.37	0.12648
256.63	150.70	48.67	42.395	20.27	7.7659	5.38	0.12664
256.64	150.67	48.14	41.723	20.28	7.7866	5.38	0.12708
252.49	150.01	48.17	41.768	20.28	7.7918	5.25	0.11747
252.62	150.18	48.16	41.762	19.81	7.3540	5.25	0.11869
252.62	150.10	47.63	41.077	19.82	7.3927	5.25	0.11884
248.48	149.37	47.66	41.126	19.80	7.3481	5.13	0.10952
248.61	149.51	47.66	41.132	19.34	6.9356	5.13	0.10936
248.59	149.50	47.13	40.445	19.35	6.9582	5.13	0.11049
244.46	148.52	47.15	40.486	19.34	6.9358	5.01	0.10157
244.57	148.71	47.15	40.493	18.88	6.5373	5.01	9.9880×10^{-2}
244.57	148.83	46.62	39.810	18.89	6.5427	5.01	9.9880×10^{-2}
240.45	147.78	46.64	39.857	18.89	6.5436	4.89	9.2890×10^{-2}
240.54	147.84	46.64	39.840	18.45	6.1579	4.89	9.2690×10^{-2}
240.54	147.89	46.11	39.162	18.45	6.1755	4.89	9.2930×10^{-2}
236.41	146.85	46.14	39.196	18.44	6.1673	4.77	8.5980×10^{-2}
236.51	147.02	46.14	39.195	18.00	5.8038	4.77	8.6130×10^{-2}
236.52	146.91	45.61	38.528	18.02	5.8147	4.77	8.6140×10^{-2}
232.38	145.84	45.63	38.551	18.02	5.8141	4.66	7.9830×10^{-2}

DOI: 10.1021/acs.inorgchem.7b00462
Inorg. Chem. 2017, 56, 5839−5850

Table 6. continued

T (K)	$C_{p,m}$ (J K^{-1} mol^{-1})	T (K)	$C_{p,m}$ (J K^{-1} mol^{-1})	T (K)	$C_{p,m}$ (J K^{-1} mol^{-1})	T (K)	$C_{p,m}$ (J K^{-1} mol^{-1})
232.49	145.96	45.63	38.555	17.59	5.4622	4.66	7.9230×10^{-2}
232.48	146.02	45.10	37.870	17.60	5.4785	4.66	7.9820×10^{-2}
228.37	145.08	45.12	37.912	17.59	5.4739	4.55	7.3160×10^{-2}
228.46	145.10	45.12	37.900	17.18	5.1504	4.55	7.5280×10^{-2}
228.46	145.05	44.59	37.224	17.19	5.1550	4.55	7.4780×10^{-2}
224.34	144.24	44.62	37.256	17.18	5.1531	4.43	6.9070×10^{-2}
224.43	144.37	44.62	37.253	16.78	4.8408	4.44	6.8680×10^{-2}
224.45	144.34	44.09	36.556	16.78	4.8519	4.44	6.8210×10^{-2}
220.32	143.30	44.11	36.599	16.78	4.8467	4.33	6.4690×10^{-2}
220.41	143.41	44.11	36.593	16.38	4.5597	4.34	6.3390×10^{-2}
220.41	143.31	43.58	35.903	16.39	4.5603	4.33	6.5490×10^{-2}
216.30	142.33	43.60	35.944	16.38	4.5552	4.23	5.9750×10^{-2}
216.38	142.31	43.60	35.937	15.99	4.2725	4.24	6.0840×10^{-2}
216.38	142.39	43.07	35.257	16.01	4.2816	4.23	5.9510×10^{-2}
212.25	141.24	43.10	35.298	16.00	4.2775	4.13	5.5180×10^{-2}
212.35	141.40	43.09	35.283	15.62	4.0126	4.13	5.5460×10^{-2}
212.35	141.41	42.57	34.597	15.63	4.0163	4.13	5.5940×10^{-2}
208.24	140.15	42.59	34.632	15.62	4.0155	4.04	5.2470×10^{-2}
208.31	140.22	42.59	34.626	15.25	3.7646	4.04	5.1320×10^{-2}
208.31	140.24	42.06	33.939	15.26	3.7745	4.04	5.1380×10^{-2}
204.21	139.07	42.08	33.967	15.26	3.7716	3.94	4.7470×10^{-2}
204.28	139.22	42.08	33.973	14.89	3.5300	3.94	4.7740×10^{-2}
204.28	139.20	41.55	33.272	14.91	3.5349	3.94	4.7650×10^{-2}
200.18	138.00	41.57	33.311	14.90	3.5374	3.85	4.4080×10^{-2}
200.25	138.06	41.57	33.301	14.54	3.3081	3.85	4.4050×10^{-2}
200.26	138.04	41.05	32.619	14.55	3.3117	3.85	4.4260×10^{-2}
196.14	136.81	41.07	32.660	14.55	3.3141	3.76	4.1200×10^{-2}
196.22	136.92	41.06	32.644	14.20	3.0947	3.76	4.0950×10^{-2}
196.22	136.94	40.54	31.957	14.21	3.1007	3.76	4.0910×10^{-2}
192.11	135.68	40.56	31.988	14.21	3.0987	3.67	3.8110×10^{-2}
192.18	135.77	40.56	31.994	13.86	2.8953	3.67	3.8120×10^{-2}
192.18	135.71	40.03	31.302	13.88	2.9021	3.67	3.7950×10^{-2}
188.08	134.47	40.05	31.333	13.88	2.9038	3.58	3.5360×10^{-2}
188.15	134.52	40.05	31.327	13.54	2.7124	3.58	3.5480×10^{-2}
188.15	134.53	39.53	30.648	13.55	2.7109	3.59	3.4990×10^{-2}
184.05	133.29	39.55	30.675	13.55	2.7155	3.50	3.2930×10^{-2}
184.12	133.26	39.54	30.670	13.22	2.5316	3.50	3.3200×10^{-2}
184.12	133.26	39.02	29.987	13.23	2.5347	3.50	3.3020×10^{-2}
180.04	132.01	39.04	30.021	13.23	2.5353	3.42	3.0580×10^{-2}
180.08	132.13	39.04	30.024	12.91	2.3572	3.42	3.0950×10^{-2}
180.09	132.04	38.51	29.340	12.92	2.3644	3.42	3.1160×10^{-2}
176.01	130.65	38.53	29.374	12.93	2.3676	3.34	2.8860×10^{-2}
176.07	130.70	38.53	29.372	12.61	2.2034	3.34	2.8800×10^{-2}
176.06	130.71	38.01	28.672	12.62	2.2060	3.34	2.8840×10^{-2}
171.98	129.24	38.03	28.718	12.62	2.2045	3.26	2.6860×10^{-2}
172.03	129.28	38.02	28.704	12.32	2.0549	3.26	2.6890×10^{-2}
172.03	129.36	37.50	28.029	12.33	2.0561	3.26	2.6860×10^{-2}
167.95	127.94	37.52	28.062	12.33	2.0611	3.18	2.4880×10^{-2}
167.99	127.95	37.52	28.053	12.03	1.9146	3.18	2.4850×10^{-2}
167.98	127.97	36.99	27.374	12.03	1.9176	3.19	2.5250×10^{-2}
163.91	126.51	37.01	27.396	12.03	1.9171	3.11	2.3250×10^{-2}
163.95	126.51	37.01	27.398	11.74	1.7803	3.11	2.3450×10^{-2}
163.95	126.51	36.49	26.708	11.75	1.7835	3.11	2.3410×10^{-2}
159.88	125.01	36.51	26.736	11.76	1.7871	3.04	2.1950×10^{-2}
159.91	125.04	36.51	26.723	11.47	1.6552	3.04	2.1950×10^{-2}
159.91	124.98	35.98	26.043	11.48	1.6578	3.04	2.2000×10^{-2}
155.84	123.36	36.00	26.083	11.48	1.6579	2.97	2.0570×10^{-2}
155.86	123.45	36.00	26.073	11.20	1.5402	2.97	2.0520×10^{-2}
155.86	123.41	35.47	25.373	11.21	1.5428	2.97	2.0350×10^{-2}
151.80	121.75	35.49	25.428	11.21	1.5440	2.90	1.9310×10^{-2}
151.82	121.69	35.49	25.405	10.94	1.4302	2.90	1.9280×10^{-2}

DOI: 10.1021/acs.inorgchem.7b00462
Inorg. Chem. 2017, 56, 5839−5850

Table 6. continued

T (K)	$C_{p,m}$ (J K^{-1} mol^{-1})	T (K)	$C_{p,m}$ (J K^{-1} mol^{-1})	T (K)	$C_{p,m}$ (J K^{-1} mol^{-1})	T (K)	$C_{p,m}$ (J K^{-1} mol^{-1})
151.82	121.73	34.97	24.741	10.95	1.4306	2.90	1.9470×10^{-2}
147.77	120.09	34.99	24.771	10.95	1.4322	2.83	1.5950×10^{-2}
147.79	120.08	34.98	24.758	10.68	1.3259	2.84	1.6010×10^{-2}
147.78	120.10	34.46	24.083	10.69	1.3300	2.84	1.6110×10^{-2}
143.72	118.36	34.48	24.123	10.69	1.3315	2.77	1.5000×10^{-2}
143.74	118.34	34.48	24.103	10.44	1.2310	2.77	1.4920×10^{-2}
143.74	118.34	33.95	23.439	10.44	1.2313	2.77	1.4920×10^{-2}
139.68	116.38	33.98	23.462	10.44	1.2311	2.70	1.4020×10^{-2}
139.70	116.40	33.97	23.458	10.19	1.1384	2.70	1.3910×10^{-2}
139.70	116.34	33.45	22.780	10.20	1.1408	2.70	1.3920×10^{-2}
135.65	114.34	33.47	22.821	10.20	1.1419	2.64	1.3010×10^{-2}
135.66	114.35	33.47	22.802	9.96	1.0551	2.64	1.2920×10^{-2}
135.66	114.31	32.95	22.152	9.96	1.0561	2.64	1.2950×10^{-2}
131.61	112.28	32.96	22.160	9.96	1.0556	2.57	1.2100×10^{-2}
131.62	112.26	32.96	22.171	9.72	0.97401	2.57	1.2060×10^{-2}
131.62	112.24	32.44	21.504	9.73	0.97647	2.57	1.1990×10^{-2}
127.57	110.10	32.46	21.535	9.73	0.97672	2.52	1.1270×10^{-2}
127.57	110.10	32.45	21.528	9.49	0.90085	2.52	1.1280×10^{-2}
127.57	110.07	31.94	20.870	9.50	0.90027	2.52	1.1220×10^{-2}
123.53	107.89	31.95	20.889	9.50	0.90100	2.46	1.0530×10^{-2}
123.54	107.84	31.95	20.889	9.26	0.83045	2.46	1.0520×10^{-2}
123.54	107.87	31.43	20.234	9.28	0.83169	2.45	1.0470×10^{-2}
119.50	105.45	31.44	20.255	9.28	0.83279	2.40	9.8700×10^{-3}
119.49	105.44	31.44	20.243	9.04	0.76799	2.40	9.7700×10^{-3}
119.49	105.39	30.92	19.595	9.05	0.76806	2.40	9.8000×10^{-3}
115.45	103.00	30.94	19.608	9.05	0.76923	2.34	9.2100×10^{-3}
115.45	102.98	30.94	19.614	8.83	0.70691	2.34	9.1500×10^{-3}
115.45	103.04	30.42	18.957	8.84	0.70762	2.34	9.1500×10^{-3}
111.41	100.48	30.43	18.977	8.84	0.70842	2.29	8.5700×10^{-3}
111.39	100.46	30.43	18.980	8.63	0.65315	2.29	8.5500×10^{-3}
111.40	100.52	29.91	18.341	8.63	0.65340	2.29	8.5400×10^{-3}
107.35	97.856	29.92	18.351	8.63	0.65412	2.24	7.9200×10^{-3}
107.35	97.839	29.92	18.341	8.42	0.60171	2.24	7.9300×10^{-3}
107.34	97.805	29.39	17.716	8.43	0.60040	2.23	7.9100×10^{-3}
103.30	95.053	29.42	17.736	8.43	0.60089	2.18	7.4100×10^{-3}
103.30	95.047	29.41	17.722	8.23	0.55410	2.18	7.3900×10^{-3}
103.30	95.013	28.89	17.095	8.23	0.55396	2.18	7.3700×10^{-3}
99.25	92.193	28.91	17.120	8.23	0.55480	2.14	6.8700×10^{-3}
99.25	92.172	28.90	17.110	8.03	0.51232	2.14	6.8600×10^{-3}
99.25	92.192	28.39	16.504	8.04	0.51177	2.14	6.8500×10^{-3}
95.21	89.272	28.39	16.497	8.04	0.51178	2.09	6.3900×10^{-3}
95.20	89.273	28.40	16.507	7.84	0.47083	2.09	6.3700×10^{-3}
95.21	89.216	27.89	15.901	7.85	0.47006	2.09	6.3500×10^{-3}
91.16	86.179	27.89	15.903	7.85	0.47040	2.03	5.9000×10^{-3}
91.15	86.104	27.89	15.916	7.66	0.43254	2.03	5.8700×10^{-3}
91.16	86.112	27.38	15.285	7.67	0.43328	2.04	5.9200×10^{-3}
87.11	82.901	27.38	15.304	7.67	0.43355		

the temperature range T = 2.0−20.3 K. The corresponding coefficients are given in Table 4. In addition, the use of a linear δT term appeared necessary to describe the experimental curve of K_2NpO_4. More recently, the occurrence of such a linear term was also reported in Na_4NpO_5,[36] which was related to the presence of defects within the material and an asymmetric peak profile shape in opposite directions for successive *hkl* reflections clearly visible on the X-ray diffraction pattern. The X-ray diffraction data of K_2NpO_4 do not show such features, however. Self-heating effects coming from the radioactive decay of ^{237}Np were considered but appeared negligible. Moreover, departure from stoichiometry is unlikely according to the present Np-L_3 XANES results and Mössbauer data of ref 8. Hence, the physical origin of this feature remains unclear. The appearance of a nuclear Schottky effect arising from the magnetic hyperfine splitting interaction between the unpaired 5f electron and the magnetic moment at the Np nucleus (I = 5/2) was suggested for Na_2NpO_4, as the corresponding data showed a reincrease below 3.7 K.[37] K_2NpO_4 might show similar behavior (Figure 7), but we cannot conclude in the absence of data below 2.0 K, which would require complementary measurements using a ^3He refrigerator.

DOI: 10.1021/acs.inorgchem.7b00462
Inorg. Chem. 2017, 56, 5839−5850

CONCLUSION

A Rietveld refinement of the crystal structure of K_2NpO_4, tetragonal in space group $I4/mmm$, is reported for the first time in the present work. The refined cell parameters and bond lengths are in good agreement with the trend of decreasing ionic radii along the actinide series. XANES data have also been collected at the Np-L_3 edge, which have confirmed the hexavalent state of neptunium in this compound and therefore the assigned stoichiometry. The measured absorption edge threshold E_0 fits very well the linear correlation observed for the sodium neptunates between E_0 and the isomer shift value δ_{IS} measured by Mössbauer spectroscopy. Moreover, double-peak white lines have been observed for K_2NpO_4, which are usually attributed to multiple scattering resonances of the actinyl compounds, but the interpretation could be more intricate. Electronic density calculations are needed to obtain more insight into those complex features.

Low-temperature heat capacity data have been collected in the temperature range T = 2.1−298.4 K for K_2NpO_4 and T = 2.0−312.4 K for K_2UO_4, and the standard entropy and heat capacity of both compounds have been derived at 298.15 K. The latter data have revealed the presence of an anomaly at 25.9 K with an associated magnetic entropy S_{mag} = 3.1 ± 0.1 J K^{-1} mol^{-1}, which most probably corresponds to the magnetic hyperfine splitting event observed in the literature by Mössbauer spectroscopy at a slightly lower temperature: i.e., T = 19.5(5) K.[8] Both the present low-temperature heat capacity data and the magnetic susceptibility measurements of Nectoux et al.[8] are consistent with the hypothesis of a ferromagnetic ordering transition around T = 25.9 K. Complementary studies involving repeated Mössbauer spectroscopy and magnetic susceptibility measurements, as well as neutron diffraction measurements on a well-characterized material, would allow confirmation of those results. Finally, the amplitude of the anomaly at 25.9 K is smaller than expected for this Kramers system ($S_{mag} = R \ln 2$), but similar results have also been reported for α-Na_2NpO_4. The low values of the ordered moment derived from the Mössbauer data (~0.6 μ_B), of the paramagnetic effective moment derived from the magnetic susceptibility data (μ_{eff} = 1.37 μ_B), and of the magnetic entropy ($S_{mag} = 0.538R \ln 2$), are not unusual for $5f^1$ systems. Further investigations involving spectroscopy measurements at low energy and theoretical calculations are clearly required to get further insight into the Np(VI) crystal-field ground state and magnetic behavior of the alkali and alkaline-earth neptunates.

APPENDIX

Experimental heat capacity data for K_2NpO_4 and K_2UO_4 are given in Tables 5 and 6.

ASSOCIATED CONTENT

Supporting Information

The Supporting Information is available free of charge on the ACS Publications website at DOI: 10.1021/acs.inorgchem.7b00462.

X-ray crystallographic file of K_2NpO_4 (CIF)
X-ray crystallographic file of K_2UO_4 (CIF)
X-ray diffraction pattern and refined atomic positions for K_2UO_4 (PDF)

AUTHOR INFORMATION

Corresponding Author

*E-mail for A.L.S.: a.l.smith@tudelft.nl.

ORCID

Anna L. Smith: 0000-0002-0355-5859
Andreas C. Scheinost: 0000-0002-6608-5428
Anthony K. Cheetham: 0000-0003-1518-4845

Notes

The authors declare no competing financial interest.

ACKNOWLEDGMENTS

The authors thank D. Bouëxière for the collection of the X-ray diffraction data. The authors acknowledge the 7th Framework Program of the European Commission. XAS experiments at the ESRF have been supported by the European FP7 TALISMAN project, under contract with the European Commission. The authors thank TALISMAN and the ESRF for provision of beam time.

REFERENCES

(1) Yoshida, Z.; Johnson, S. G.; Kimura, T.; Krsul, J. R. In *The Chemistry of the Actinide and Transactinide Elements*; Morss, L. R., Edelstein, N., Fuger, J., Katz, J. J., Eds.; Springer: Berlin, 2006; Chapter 6 (Neptunium), pp 699−812.

(2) Bickel, M.; Kanellakopulos, B. Systematics in the Magnetic Properties of Ternary Actinoid Oxides. *J. Solid State Chem.* **1993**, *107*, 273−284.

(3) Santini, P.; Carretta, S.; Amoretti, G.; Caciuffo, R.; Magnani, N.; Lander, G. H. Multipolar interactions in f-electron systems: The paradigm of actinide dioxides. *Rev. Mod. Phys.* **2009**, *81*, 807−864.

(4) Smith, A. L.; Raison, P. E.; Martel, L.; Prieur, D.; Charpentier, T.; Wallez, G.; Suard, E.; Scheinost, A. C.; Hennig, C.; Martin, P.; Kvashnina, K. O.; Cheetham, A. K.; Konings, R. J. M. A New Look at the Structural Properties of Trisodium Uranate Na_3UO_4. *Inorg. Chem.* **2015**, *54*, 3552−3561.

(5) Smith, A. L.; Raison, P. E.; Hen, A.; Bykov, D.; Colineau, E.; Sanchez, J.-P.; Konings, R. J. M.; Cheetham, A. K. Structural investigation of Na_3NpO_4 and Na_3PuO_4 using X-ray diffraction and ^{237}Np Mössbauer spectroscopy. *Dalton Transactions* **2015**, *44*, 18370−18377.

(6) Smith, A. L.; Hen, A.; Raison, P. E.; Colineau, E.; Griveau, J.-C.; Magnani, N.; Sanchez, J.-P.; Konings, R. J. M.; Caciuffo, R.; Cheetham, A. K. X-ray Diffraction, Mössbauer Spectroscopy, Magnetic Susceptibility, and Specific Heat Investigations of Na_4NpO_5 and Na_5NpO_6. *Inorg. Chem.* **2015**, *54*, 4556−4564.

(7) Smith, A. L.; Hen, A.; Magnani, N.; Sanchez, J.-P.; Colineau, E.; Griveau, J.-C.; Raison, P. E.; Caciuffo, R.; Konings, R. J. M.; Cheetham, A. K. Mössbauer spectroscopy, magnetization, magnetic susceptibility, and low temperature heat capacity of α-Na_2NpO_4. *J. Phys.: Condens. Matter* **2016**, *28*, 086002.

(8) Nectoux, F.; Jové, J.; Cousson, A.; Pagès, M.; Gal, J. First order magnetic transition in the tetragonal K_2NpO_4. *J. Magn. Magn. Mater.* **1981**, *24*, L113−L116.

(9) Butorin, S. M.; Kvashnina, K. O.; Smith, A. L.; Popa, K.; Martin, P. M. Crystal-Field and Covalency Effects in Uranates: An X-Ray Spectroscopic Study. *Chem. - Eur. J.* **2016**, *22*, 9693−9698.

(10) Smith, A. L.; Martin, P.; Prieur, D.; Scheinost, A. C.; Raison, P. E.; Cheetham, A. K.; Konings, R. J. M. Structural Properties and Charge Distribution of the Sodium Uranium, Neptunium, and Plutonium Ternary Oxides: A Combined X-ray Diffraction and XANES Study. *Inorg. Chem.* **2016**, *55* (4), 1569−1579.

(11) Unger, L. M.; Trubey, D. K. *Specific Gamma-Ray Dose Constants for Nuclides Important to Dosimetry and Radiological Assessment, ORNL/RSIC-45/RI*, 1982; DOI: 10.2172/5158466

(12) Rodriguez-Carvajal, J. Recent advances in magnetic structure determination by neutron powder diffraction. *Phys. B* **1993**, *192*, 55−69.

(13) Matz, W.; et al. ROBL - a CRG beamline for radiochemistry and materials research at the ESRF. *J. Synchrotron Radiat.* **1999**, *6*, 1076−1085.

DOI: 10.1021/acs.inorgchem.7b00462
Inorg. Chem. 2017, 56, 5839−5850

(14) Ravel, B.; Newville, M. ATHENA, ARTEMIS, HEPHAESTUS: data analysis for X-ray absorption spectroscopy using IFEFFIT. *J. Synchrotron Radiat.* **2005**, *12*, 537−541.
(15) Lashley, J. C.; et al. Critical examination of heat capacity measurements made on a Quantum Design physical property measurement system. *Cryogenics* **2003**, *43*, 369−378.
(16) Javorský, P.; Wastin, F.; Colineau, E.; Rebizant, J.; Boulet, P.; Stewart, G. Low-temperature heat capacity measurements on encapsulated transuranium samples. *J. Nucl. Mater.* **2005**, *344*, 50−55.
(17) Roof, I. P.; Smith, M. D.; zur Loye, H.-C. Crystal growth of K_2UO_4 and Na_4UO_5 using hydroxide fluxes. *J. Cryst. Growth* **2010**, *312*, 1240−1243.
(18) Smith, A. L.; Raison, P. E.; Konings, R. J. M. Synthesis and crystal structure characterisation of sodium neptunate compounds. *J. Nucl. Mater.* **2011**, *413*, 114−121.
(19) Appel, H.; Bickel, M.; Melchior, S.; Kanellakopulos, B. Structural and magnetic properties of $BaUO_4$ and $BaNpO_4$. *J. Less-Common Met.* **1990**, *162*, 323−334.
(20) Bertram, S.; Kaindl, G.; Jové, J.; Pagès, M.; Gal, J. Electronic structure of actinide compounds from the L_{III}-edge X-ray absorption. *Phys. Rev. Lett.* **1989**, *63*, 2680−2683.
(21) Bertram, S.; Kaindl, G.; Jové, J.; Pagès, M. L-Edge X-Ray Absorption Studies of Neptunium Compounds. *Phys. B* **1989**, *158*, 508−510.
(22) Antonio, M.; Soderholm, L. In *The Chemistry of the Actinide and Transactinide Elements*; Morss, L. R., Edelstein, N., Fuger, J., Katz, J. J., Eds.; 2006; Chapter 28 (X-ray absorption spectroscopy of the actinides), pp 3086−3198.
(23) Westrum, E. F. J.; Hatcher, J. B.; Osborne, D. W. The Entropy and Low Temperature Heat Capacity of Neptunium Dioxide. *J. Chem. Phys.* **1953**, *21*, 419−423.
(24) Magnani, N.; Santini, P.; Amoretti, G.; Caciuffo, R.; Javorsky, P.; Wastin, F.; Rebizant, J.; Lander, G. H. Octupolar order in NpO_2: A specific heat investigation. *Phys. B* **2005**, *359*−*361*, 1087−1089.
(25) Santini, P.; Carretta, S.; Magnani, N.; Amoretti, G.; Caciuffo, R. Hidden Order and Low-Energy Excitations in NpO_2. *Phys. Rev. Lett.* **2006**, *97*, 207203.
(26) Dickson, D. P. E.; Berry, F. J. *Mössbauer spectroscopy*; Cambridge University Press: New York, 2005.
(27) Tabuteau, A.; Jové, J.; Pagès, M.; Novion, C. H.; Gal, J. Mössbauer and magnetization studies of the $U_{1-x}Np_xO_2$ fluorites. *Solid State Commun.* **1984**, *50*, 357−361.
(28) Majzlan, J.; Navrotsky, A.; Woodfield, B. F.; Lang, B. E.; Boerio-Goates, J.; Fisher, R. A. Phonon, Spin-Wave, and Defect Contributions. *J. Low Temp. Phys.* **2003**, *130*, 69−76.
(29) Woodfield, B. F.; Boerio-Goates, J.; Shapiro, J. L.; Putnam, R. L.; Navrotsky, A. Molar heat capacity and thermodynamic functions of zirconolite $CaZrTi_2O_7$. *J. Chem. Thermodyn.* **1999**, *31*, 245−253.
(30) Woodfield, B. F.; Shapiro, J. L.; Stevens, R.; Boerio-Goates, J.; Putnam, R. L.; Helean, K. B.; Navrotsky, A. Molar heat capacity and thermodynamic functions for $CaTiO_3$. *J. Chem. Thermodyn.* **1999**, *31*, 1573−1583.
(31) Smith, S. J.; Stevens, R.; Liu, S.; Li, G.; Navrotsky, A.; Boerio-Goates, J.; Wooodfield, B. F. Heat capacities and thermodynamic functions of TiO_2 anatase and rutile: Analysis of phase stability. *Am. Mineral.* **2009**, *94*, 236−243.
(32) Swalin, R. A. *Thermodynamics of Solids*, 1st ed.; Wiley: New York, 1962.
(33) Gopal, E. S. *Specific heats at low temperatures*; Plenum Press: New York, 1966.
(34) Shi, Q.; Zhang, L.; Schlesinger, M. E.; Boerio-Goates, J.; Woodfield, B. F. Low temperature heat capacity Study of $Fe(PO_3)_3$ and $Fe_2P_2O_7$. *J. Chem. Thermodyn.* **2013**, *61*, 51−57.
(35) Shi, Q.; Park, T.-J.; Schliesser, J.; Navrotsky, A.; Woodfield, B. F. Low temperature heat capacity study of Ba_2TiSiO_8 and Sr_2TiSiO_8. *J. Chem. Thermodyn.* **2014**, *72*, 77−84.
(36) Smith, A. L.; Griveau, J.-C.; Colineau, E.; Raison, P. E.; Wallez, G.; Konings, R. J. M. Low temperature heat capacity of Na_4UO_5 and Na_4NpO_5. *J. Chem. Thermodyn.* **2015**, *91*, 245−255.
(37) Smith, A. L.; Griveau, J.-C.; Colineau, E.; Raison, P. E.; Konings, R. J. M. Low temperature heat capacity of α-Na_2NpO_4. *Thermochim. Acta* **2015**, *617*, 129−135.

DOI: 10.1021/acs.inorgchem.7b00462
Inorg. Chem. 2017, 56, 5839−5850